International Journal of Rock Mechanics & Mining Sciences 148 (2021) 104965

Contents lists available at ScienceDirect

International Journal of Rock Mechanics and Mining Sciences

journal homepage: www.elsevier.com/locate/ijrmms

Modeling the behavior of a coal pillar rib using Bonded Block Models with emphasis on ground-support interaction

Sankhaneel Sinha *, Gabriel Walton

Department of Geology and Geological Engineering, Colorado School of Mines, 1516 Illinois St, Golden, CO, USA

ARTICLE INFO

Keywords:
Bonded block models
Coal pillar
Rock fracturing
Reinforcement
Voronoi tessellation

ABSTRACT

Rib spalling is a major hazard in the mining industry and in absence of coal rib support guidelines, accidents have continued to occur in recent years. Developing effective support guidelines requires a complete understanding of pillar damage mechanisms as well as the rock-support interaction mechanism. Bonded Block Models (BBMs) represent a convenient tool for this purpose, as they can reproduce the rock fracturing process reasonably well, but it is not known whether this modeling technique can quantitatively replicate the impact of reinforcement (bolts) on otherwise unsupported ground. To bridge this gap in research, we employed the BBM approach to simulate the behavior of a supported coal pillar rib located in a longwall mine in Australia. This case study presents a unique opportunity in that two otherwise identical chain pillars with different support densities adjacent to one another were instrumented. After calibrating a model against displacement and stress measurements made over the course of mining in one pillar, the support in the calibrated BBM was modified to match that of the adjacent chain pillar. This model could predict the rib displacement to within 6 mm of what was measured in-situ. Given the ability of the BBM to match field-measured displacements and stresses and also field observations for varying support densities, it seems that such a model has the potential to aid in the development of a support design tool. Lastly, the effect of block shape was investigated by replacing the elongated blocks with isotropic polygonal blocks. This model could not reproduce the ground-support interaction very well, likely due to the inaccurate geometric representation of an anisotropic rock like coal.

1. Introduction

Recent years have seen a rapid increase in the use of discontinuum modeling tools for studying the rock fracturing process, both at the laboratory-scale[1–5] and at the field-scale.[6–10] In comparison to the continuum approach, where material damage is approximated through inelastic yield, discontinuum models attempt to explicitly simulate the rock fracturing process by allowing the elements to detach and separate. More recently, discontinuum models have been shown to better replicate the ground-support interaction mechanism in comparison to continuum models and therefore have the potential to be used as a support design tool.[11,12] The necessity for developing such tools is highlighted by the fact that current support design approaches are based mostly on site-specific experience rather than a more generally applicable scientific basis.[13–15]

While a number of discontinuum modeling techniques exist (PFC^{2D}:[16–18]; FDEM:[19-21], etc.), this study is focused on the Bonded Block Modeling (BBM) method as implemented in Itasca's Universal Distinct Element Code (UDEC). In BBMs, a material space is represented by bonded polygonal (Voronoi Tessellation) or triangular (Trigon) blocks that can detach along the contacts when the tensile and/or shear strength of the contact is exceeded. Although the vast majority of the previous studies have focused on laboratory-scale rock fracturing process, there has been some success in reproducing field-scale behaviors as well. Coggan et al.[6] and Gao and Stead[8] modeled the shear fracture formation above coal mine entries, while Gao et al.[22] simulated the longwall caving process. Christianson et al.[23] conducted numerical triaxial tests on lithophysical tuff specimens using Voronoi blocks to aid in the design of the Yucca mountain nuclear waste repository. Preston et al.[24] investigated the effect of aspect ratio (i.e. width to height ratio) on the strength of a limestone pillar. Muaka et al.[25] used an integrated discrete fracture network (DFN) – Voronoi approach to understand the destabilizing effect of clay-filled shear structure on the stability of rock pillars. While both Voronoi and Trigons have been used in field-scale applications, Sinha and Walton[12] have recently shown that unlike Voronoi, Trigon models tend to show less of a reduction in bulking when

* Corresponding author.
E-mail address: sankhaneelsinha@mines.edu (S. Sinha).

https://doi.org/10.1016/j.ijrmms.2021.104965
Received 4 March 2021; Received in revised form 26 July 2021; Accepted 30 October 2021
Available online 3 November 2021

supports are added than would be expected in field (at least for two-dimensional models). Accordingly, we only considered the polygonal block geometry in this study.

Coal is a brittle, anisotropic material, and its mechanical response is largely controlled by its cleat structure (face and butt cleats, with the former more connected than the latter in general).[26,27] As cleats are natural planes of weakness, their orientation with respect to the roadway influences the ground control issues observed at a site.[28,29] Gao et al.[22] modeled the anisotropic behavior of coal in PFC^{3D} by representing the coal matrix using bonded spheres and the cleats and bedding using a DFN. A similar approach was applied by Vardar et al.[30] where the coal matrix was simulated using Trigons in 2D and the cleats were simulated using a DFN. In terms of actual coal mine case studies, Bai et al.[9] used Voronoi to simulate the behavior of an entry housed in a water-rich environment. Other notable works include those by Kang et al.,[31] Chen et al.,[32] and Yang et al.[33] using the Trigon modeling approach. However, none of these coal-mine case studies considered cleats and/or their effect on roadway deformations. To allow fractures to form and propagate preferentially along the direction of face cleats (as reported by Colwell[14] for the site under consideration), we use elongated Voronoi blocks to model coal, similar to the approach adopted by Ghazvinian et al.[34] and Zhu et al.[64] Anisotropic behavior cannot be obtained using regular Voronoi blocks as this shape is isotropic with respect to the coordinate axes. The representation of a coal pillar using elongated Voronoi blocks is based on three major assumptions: (1) Small-scale heterogeneities in the coal do not affect the macroscopic behavior of the pillar; (2) Cleats primarily act as weakness planes rather than pre-existing discontinuities; and (3) There are no significant large-scale joints that affect the coal pillar behavior. For the site under consideration, no significant jointing or micro-scale heterogeneity in the coal was reported.[14] Note that while the application of the BBM method is not novel in and of itself, the use of elongated blocks for simulating damage in a supported pillar is.

Scientific research to improve the performance of such coal pillar ribs, particularly through the use of support, has been ongoing for several decades.[14,28,35–39] More recent endeavors by National Institute of Occupational Safety and Health (NIOSH) researchers have focused on minimizing rib hazard using numerical and/or empirical approaches[40–43] and novel techniques like seismic monitoring[44] and photogrammetry.[45] Despite these advances in our knowledge of pillar damage mechanisms and the rock-support interaction, rib-failure-related fatalities in underground coal mines have continued to occur. For example, among incidents classified as “fall of face, rib or pillar”, the average fatality rate was 1.3 per year for 1996–2012 and about 40–50 injuries occurred every year from 2013 to 2017 in the United States.[46] These ongoing issues highlight the need for the development of a robust tool that can be used for the effective design of ground supports in a wide variety of mining situations.

The current study is a continuation of the authors’ efforts to better understand the capabilities of BBM, extend its application to large structure analysis, and utilize it in the development of a skin support design tool for use in underground mines.[12,47] Specifically, this study is focused on modeling the West Cliff mine case study,[14] which is unique in the sense that two adjacent pillars were instrumented, but the pillars had different rib support patterns. Given the proximity of the two pillars and the fact that both were given a single geological description by Colwell,[14] the two pillars can be considered similar from a geological perspective, and any differences in the observed behavior can be directly linked to the differing support patterns.

The West Cliff mine case study was previously modeled by Mohamed et al.[41] and Sinha and Walton[48] in FLAC^{3D}. Mohamed et al.[41] used a user-defined coal rib constitutive model while Sinha and Walton[48] employed the progressive S-shaped yield criterion.[49] Subsequently, Sinha and Walton[12] tested the calibrated continuum FLAC^{3D} model with the addition of extra bolts (above and beyond those installed in the field) and showed that the incorporation of extra bolts suppressed the rib displacements by no more than 7%. In contrast, the rib displacement measured at the second pillar (with 2 extra bolts) was only ~30% (70% reduction) of that at the pillar to which the model was calibrated. This previous finding indicates that continuum models have difficulty in directly reproducing the effect of reinforcement on highly dilatant ground behavior. More discussion on this topic can be found in Sinha and Walton.[12]

Since continuum models maintain strain continuity within their domain, the use of discontinuum models is often preferable in scenarios where sliding and opening along existing joint sets and/or fracturing of intact rock material play a dominant role in rockmass deformation.[50–52] Although some continuum modeling studies using ubiquitous joints[53–55] have simulated large changes in roof deformation with incorporation of supports, their potential to simulate the support effect quantitatively in pillar ribs is yet to be established. With all that in mind, in this study we demonstrate that BBMs can replicate the local reinforcement influence on ground behavior at the West Cliff mine. Specifically, we calibrated the behavior of a coal pillar in the West Cliff mine against field-measured displacements and stresses and used this calibrated model to evaluate the influence of support in comparison to what was observed in-situ.

This case study ultimately provides a unique opportunity to demonstrate several important aspects of the capabilities of Bonded Block Modeling that have not been previously well-documented in the literature. These include the ability of BBMs to do the following: (1) Quantitatively reproduce the rock-support interaction behavior, (2) Capture the extent of anisotropy expected for coal through modification of the block shape, (3) Reproduce localized large-strain damage processes, which are difficult and often impossible to simulate using continuum models, and, (4) Realistically simulate the transition from highly-dilatant extensile fracturing along the pillar periphery to minimally-dilatant shear deeper within the pillar by using inelastic blocks. The practical implications of the findings of this study in context of underground mine design are presented in Section 6.

2. Site description and model setup

2.1. Description of the site and instrumentation

The West Cliff mine is a two-entry longwall coal mine located along the south-east coast of Australia. The particular panel under consideration (Panel 515) is 480 m below ground surface, with the chain pillars spaced at 42 m and 125 m center-to center across and along the long axis of the panel, respectively. At the instrumented sites, the entry was 4.8 m wide and 3 m high. Colwell[14] installed a 7 m long multi-point extensometer and a stress cell, each, in two adjacent pillars, referred to as Site

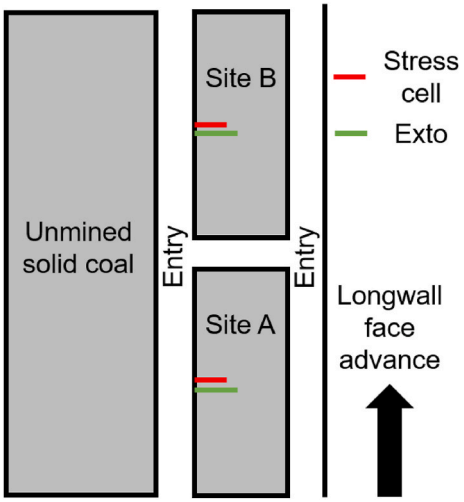

Fig. 1. Plan view of the two monitoring sites (not to scale[48]).

A and B herein (Fig. 1). Both instruments were installed horizontally at the pillar mid-height, with the stress cell located 4 m into the pillar and orientated to monitor the vertical stress changes associated with longwall face advance and progressive rib fracturing. Although the stress cells were installed when the longwall face was ~450 m inby of Site A, the extensometers were not until about the face was 72 m inby of Site A. Monitoring was continued until the longwall face was ~981 m outby of Site A.

The key difference between Sites A and B is that at Site A, the rib section was supported by two 1.2 m long, 16 mm diameter, full column resin grouted rebars while at Site B, two additional 1.8 m long rebars were installed (4 bolts in total). The 1.2 m and 1.8 m bolts were spaced at 1 m and 2 m, respectively along the entry. At both sites, some mesh was also installed – Site A had a 400 mm tall strip of mesh along the upper row of bolts while Site B had an additional 500 mm mesh along the pillar bottom. Mesh was not explicitly modeled in this study, as its effect is negligible in comparison to bolts and face plates,[39] and also because it only extended partially along the seam height, meaning that the mesh does not provide any substantial resistance to ground motion within the plane of the rockbolts. Therefore, the only type of support considered in this study is rockbolts as reinforcing elements, which serve to strengthen the rockmass and improve its self-supporting capacity.[56]

Unfortunately, the stress cell at Site B did not function properly, and model calibration was therefore conducted using the displacements and stresses measured at Site A. Once the calibration was complete, two additional 1.8 m long bolts were installed in the model and the peak rib displacement measured at Site B was compared to that in the model.

2.2. Description of the BBM setup

In the continuum models of Mohamed et al.[41] and Sinha and Walton,[48] it was assumed that the extensometers and stress cell measurements corresponded to two stages of loading: (1) Development – this corresponds to a state when the entries have relaxed completely after initial excavation; and (2) Headgate – this is related to the stress redistribution caused by the approach and passage of the adjacent longwall face. Accordingly, in these previous models, the first set of measurements by the extensometer at Site A was considered to be associated with entry relaxation, and all subsequent measurements were considered to be related to headgate loading.

While this might not be an issue for continuum models where the support elements only demonstrate strain-compatibility with the deformations of the rock[50] rather than significantly influence it, the timing of support installation is very important in discontinuum models.[57] Colwell[14] reported that the rib bolts at West Cliff mine were installed within 4 m from the face. For brittle materials like coal, entry relaxation occurs very close to the face,[41] meaning that the entries were probably fully (or almost fully) relaxed when the bolts were installed. Accordingly, the bolts were installed in the BBM after full relaxation of the entries.

In the field, the extensometers were installed after bolt installation, and the first set of measurements at −52 m face location (~12 mm rib displacement) was interpreted to be associated with the "development" condition in Mohamed et al.[41] and Sinha and Walton.[48] Given that the extensometers were installed well behind the entry face, it is likely that full entry relaxation associated with face advance had already occurred by the time the extensometers were installed. Upon recognizing this, the stress cell data at Site A were examined to evaluate whether or not this initial displacement could be associated with headgate loading.

Fig. 2a shows the vertical stress measurements made at Site A as a function of the longwall face location. It can be seen that the measured stresses do not increase until the face is about 25 m inby of the instrumented pillar, indicating that significant headgate loading had not initiated up to this point. There was also no change in rib displacement between −52 m face location and +2 m face location. Based on all this, we believe that the displacements measured in the time period between its installation at −72 m longwall face location and −52 m longwall face location were not related to development loading or headgate loading, and may correspond to time-dependent deformation mechanisms or other unknown phenomena. Since the exact cause of the displacements (~12 mm) measured at −52 m face location is not known, we considered these measurements as the baseline against which to compare all displacements associated with headgate loading and zeroed all subsequent extensometer measurements (and model results) with respect to this stage. The −25 m face location could also have been chosen as the reference point for headgate loading calculations, and such a choice does not affect the findings of this study as no stress change was observed up to the −25 m face location and no additional deformations were recorded between the −52 m and +2 m face locations. We chose the −52 m face location as the reference point for headgate loading calculations, as that is when the first set of extensometer data was recorded.

The raw displacement profiles for 5 locations of the longwall face are shown in Fig. 2b prior to zeroing relative to the −52 m face location data. Note how the depth of fracturing increased between the 58 m outby and 130 m outby face positions. The depth of significant fracturing is not always equivalent to the depth of yield, since fractures that form but do not dilate will not necessarily influence extensometer data.

Fig. 3 shows the plane strain BBM setup of a half pillar and half entry with dimensions of 21 m × 31 m that was used in this study. Only the first 4 m of the coal pillar was modeled using elongated Voronoi blocks to allow for explicit fracture formation and separation. This value was selected based on the 1–2 m depth of significant fracturing as identified from the Site A extensometer data. The rest of the coal pillar and the roof

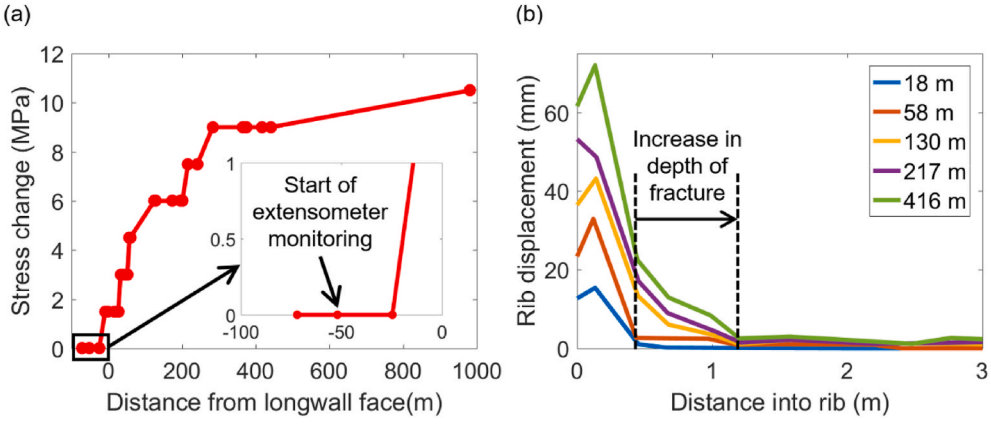

Fig. 2. (a) Vertical stress change as measured in the field with advance of the longwall face (after[41]). The inset shows a zoomed-in view of the initial portion of the graph, and has the same axis units. (b) Raw displacement profiles for 18 m, 58 m, 130 m, 217 m and 416 m outby face positions.[14]

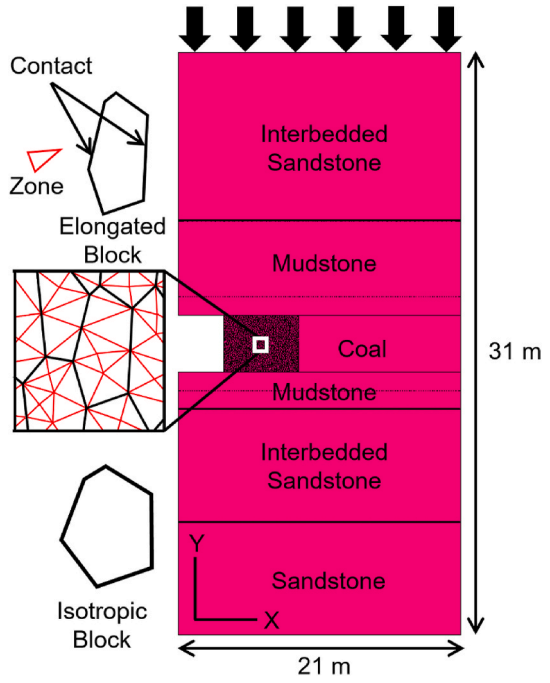

Fig. 3. Overall geometry of the BBM pillar model. The zoomed in view shows the blocks and zones. The blocks are elongated in the Y direction in 2:1 ratio. An isotropic block is also shown to allow for direct comparison between the shapes of the regular and elongated Voronoi blocks. The dashed line in the immediate roof and floor are indestructible construction joints that were used for grading the zone size away from the coal pillar.

and floor layers were modeled using continuum zones. Each Voronoi block in the pillar was discretized by multiple constant strain-triangular zones; these zones can deform elastically or inelastically depending on the constitutive model assigned to them.[58]

Sinha and Walton[59] demonstrated that it is not possible to reproduce displacements at the rib surface while also producing realistic displacements deeper into the pillar. In particular, they showed that when using elastic blocks, surficial displacements of a pillar can be matched, but if an attempt is made to match displacements at locations deeper within the pillar (~0.5 m–1 m), then it is not possible to achieve such a match without the surficial displacements being significantly overestimated. This is because of geometric mismatch that cannot be overcome for cases with blocks of limited deformability (such as fully elastic blocks). As a viable alternative, one can use an inelastic constitutive model in the zones such that damage near the pillar periphery is explicitly represented by contact failure while finer-scale damage occurring deeper within the pillar is approximated by a combination of contact failure and zone yield. A similar methodology was followed in this study, where a Cohesion-Weakening-Frictional-Strengthening model (CWFS[60]) was assigned to all zones in the coal layer (both within the Voronoi blocks and in the fully continuum portion of the pillar). The roof and floor layers were simulated as elastic, with properties listed in Table 1 (from [41]).

The CWFS strength model was initially developed for simulating brittle fracturing in rocks[60,61] and it is known that coal is a highly brittle material.[62] Although the CWFS strength model has not been directly employed for simulating coal pillars in the past, it was in part used by Sinha and Walton[48] through the application of the progressive S-shaped criterion, which essentially combines the CWFS strength model at low confinement and a shear yield model at higher confinement.[49] Since the focus of this study is on the local fracturing behavior along the pillar periphery (low-confinement conditions), only a CWFS strength model was used. If the focus were on the global strength of the pillar, then the consideration of both the low as well as the high confinement section of the progressive S-shaped criterion would have been required.

Lastly, the contacts between the coal layer and the host rock were simulated using a low strength joint element, and the corresponding properties are listed in Table 2. Such low values were selected to allow the host rock to slip along these boundaries and mimic the weakening effect of the dirt bands between the pillar and the surrounding rock as reported by Colwell.[14] All other joints within the roof and floor layers, as well as the joint between the elongated Voronoi section and the continuum zone section of the coal layer, were made indestructible (construction joints).

The most recent version of UDEC (Version 7) has the capability of generating elongated polygonal blocks using the built-in Voronoi generator, but the current study was performed in Version 6 that cannot automatically create these blocks. For that reason, a 3 m high and 12.8 m wide block had to be first built in RS2 and populated with Voronoi blocks of 0.1 m edge length, then imported into MATLAB and compressed into a 3 m × 6.4 m block (elongation factor of 2; 2.4 m entry + 4 m pillar). This procedure resulted in a 2:1 elongation in the Y direction, which is consistent with the vertical orientation of the face cleats reported by Colwell[14] at the site. The block edges were entered in UDEC as crack elements. Based on a literature review of previous field-scale BBM studies (e.g. Refs. 9,24,83,84), this 0.1 m block size is considered to be small enough so as to not impose any kinematic constraints on the fracture development process. To make the blocks deformable, each Voronoi was further discretized using zones with a maximum edge length of 0.05 m. The ratio of Voronoi edge length to zone edge length satisfies the recommendation of Fabjan et al.[85] and is larger than those used by Dadashzadeh.[86]

In these models, an elongation factor of 2 was chosen, based on some laboratory-scale unconfined compression tests (UCS) with loading at 0° and 45° to the elongation direction. We calibrated the model peak strengths to those observed in laboratory tests by Kim et al.[26] (Fig. 4), and achieved a UCS_{0^o}/UCS_{45^o} ratio of 1.38, similar to the ratio of 1.4 observed in the test data. For these models, the bottom edges were constrained via rollers and a very slow velocity was applied to the top boundaries to load the specimens. The calibrated contact parameters are listed in Table 3. Since the extent of anisotropy is controlled by the elongation factor,[63] the ability to reproduce a ratio of ~1.4 provides confidence in the chosen value. An elongation factor of 2 was also employed by Ghazvinian et al.[34] and Zhu et al.[64] to simulate laminated rocks.

While inelastic BBMs with elongated grains are complex, they represent a valid approach for modeling coal pillar ribs because they can explicitly simulate the anisotropic cleat separation process and also the transition from highly-dilatant fracturing at the periphery to minimally-dilatant shear fracturing deeper inside the pillar. In an equivalent

Table 1
Rockmass elastic parameters for different layers in the model (from [41]).

Layer	Young's Modulus (GPa)	Poisson's ratio
Interbedded sandstone (roof)	12	0.26
Mudstone (roof)	10	0.26
Coal	3	0.25
Mudstone (floor)	12	0.26
Interbedded sandstone (floor)	12	0.26
Sandstone (floor)	15	0.26

Table 2
Strength parameters for the coal-host rock interfaces.

Parameter	Peak cohesion; c_{peak} (MPa)	Residual cohesion; c_{res} (MPa)	Peak friction angle; φ_{peak} (°)	Residual friction angle; φ_{res} (°)	Tensile strength[a]; $\sigma_{t,peak}$ (MPa)
Value	0.5	0	15	15	0

[a] Residual tensile strength ($\sigma_{t,res}$) was set to 0.

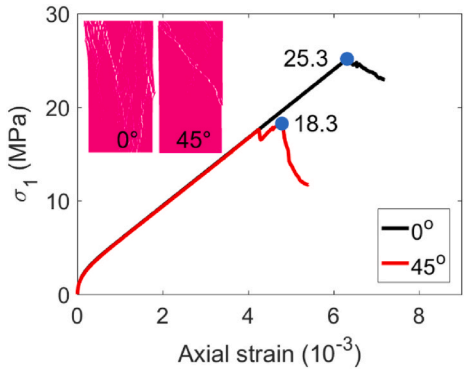

Fig. 4. Stress-strain curves for unconfined compression tests with loading along 0° and 45° to the block elongation direction. Fracture patterns post-simulation is shown in the inset.

continuum model (i.e. FLAC), anisotropy could be included in form of ubiquitous joints, but such an approach cannot fully replicate large-scale deformation processes (i.e. buckling) and adds >6 additional parameters to the matrix strength parameters. In contrast, when using a BBM, the cleat-induced anisotropy can be approximated simply by elongating the blocks.

The field-scale simulations were conducted according to the following scheme:

(a) In the first step, the model was run without any excavation until mechanical equilibrium was attained. In this step, pre-mining horizontal stresses of 3.6 MPa (in-plane) and 16.3 MPa (out-of-plane) and a vertical stress of 11.6 MPa, equivalent to the depth of mining, were applied to the model. The out-of-plane horizontal stress was based on field measurements in Colwell[14] while the in-plane horizontal stress was selected from Mohamed et al.[41] and Sinha and Walton.[48] The relative stress magnitudes are consistent with the strike-slip stress regime in and around West Cliff mine as indicated by Gale,[65] Walsh[66] and Heidbach et al.,[67] and the values of the out-of-plane and vertical stresses are close to those provided by Gale.[65] Although it is difficult to establish the value of the in-plane horizontal stress at the site with absolute certainty, the small ratio of the vertical to in-plane horizontal stress (3.6/11.6 = 0.3) is consistent with the lack of any tectonic loading along the direction of the in-plane horizontal stress.

(b) In the next step, the first 2.4 m of the entry was extracted and the unbalanced forces were relaxed in 10 stages using the built-in ZONK function. This progressive relaxation is necessary in order to avoid unrealistic yielding/fracturing along the entry due to sudden increase of unbalanced forces in the model. Once the entry was completely relaxed, rockbolts and face plates were installed in the model and all displacements were initialized to zero (i.e. with respect to the start of headgate loading).

(c) In the last step, the vertical stress along the model top boundary was increased at 0.2 MPa/stage while bringing the model to mechanical equilibrium after each stage to simulate the retreat of the longwall face. This is the same loading procedure followed by Mohamed et al.[41] and Sinha and Walton.[48] While gateroad loading is undoubtedly more complex than that considered in this study, in the absence of other pertinent information about the site, a constant stress approach was used as a simplification. A total of 35 such stages were implemented to replicate the complete stress data from Colwell.[14]

The out-of-plane stresses had no effect on zone yield during the early stages of loading (early iterations of ZONK), and by the end of the entry relaxation stage, the vertical stress (Y) increased to become the major principal stress. The X-direction stress also became the minor principal stress due to de-confinement associated with the entry. Accordingly, these two in-plane stresses were the primary factors controlling the yield/damage of the coal during the headgate loading stage.

3. Model calibration and results

3.1. Model parameters and calibration

The BBM model inputs were calibrated using an iterative manual back-analysis approach. Before delving into the results, it is necessary to review the different parameters that govern the behavior of such models. The parameters can be broadly subdivided into two categories: coal mass parameters and support parameters. The coal mass parameters can be further sub-divided into zone parameters and contact parameters. As noted previously, the CWFS strength model was applied in the model zones within the coal layer. This model requires defining Young's modulus (E), Poisson's ratio (ν), peak and residual cohesions, tensile strengths and friction angles, and a critical plastic shear strain (ε^{ps}) to control the rate of softening. As the CWFS strength model mimics the degradation of cohesion and mobilization of friction with damage (ε^{ps}), the peak cohesion is larger than the residual value, while the peak friction angle is smaller than its residual counterpart.[60,68] The same CWFS parameters were used in the Voronoi zones as well as the continuum portion of the coal seam. However, no yield was observed in the continuum portion of the coal seam after the headgate loading was complete, meaning the behavior of this portion of the pillar was effectively elastic.

Corrections in the zone modulus values are often required when separate continuum and Voronoi sections are modeled due to the presence of relatively low stiffness discontinuum contact elements in the latter.[34,69] Such corrections were not necessary in this case as the actual material being modeled is soft enough that the relative values of the contact stiffnesses used were sufficiently high to ensure that the effective modulus of the Voronoi section was the same as that of the continuum section. For the contacts, the strength parameters are similar to those for zones (c_{peak}, c_{res}, $\sigma_{t,peak}$, $\sigma_{t,res}$, φ_{peak}, φ_{res}); the normal and shear stiffness define the contact elastic behavior. The drop from peak to residual is instantaneous for the contacts.

The rockbolts were modeled using the rockbolt element available in UDEC, and the face plates were modeled using the beam structural element. All face plates were made elastic with E of 200 GPa, ν of 0.3, and a rock-to-face plate friction angle of 25°. The remainder of the rock-to-face plate interface strength properties were set to zero. Estimation of the rockbolt properties is much more difficult, as pull test data from the site was not available. There are two key parameters that govern the anchor characteristics of rockbolt elements: stiffness (K_{bond}) and cohesive strength (S_{bond}) of the grout. UDEC manual[70] provides the following equation for estimating K_{bond}:

$$K_{bond} \cong \frac{2\pi G}{10\ln(1+2t/D)} \quad (1)$$

Table 3
Contact parameters for the laboratory-scale BBM.

Parameter	c_{peak} (MPa)	c_{res} (MPa)	φ_{peak} (°)	φ_{res} (°)	$\sigma_{t,peak}$ [a] (MPa)	Normal stiffness (GPa/m/m)	Shear stiffness (GPa/m/m)
Value	14	0.5	20	7.5	1.5	500,000	250,000

[a] Residual tensile strength ($\sigma_{t,res}$) was set to 0.

where G is the grout shear modulus, D is the bolt diameter and t is the thickness of the annulus (i.e. borehole radius minus bolt radius). If the annulus of the 16 mm rockbolt was around 3–3.5 mm and the resin grout modulus is 2.25 GPa,[71] then the range of K_{bond} to be tested should be approximately 1.6–1.8 GN/m/m. Zipf[54] provided practical values of S_{bond} for simulating grouted rockbolts in different coal measure rocks. A range 120 kN/m to 150 kN/m, corresponding to grip factors of 0.3–0.4 ton/inch, was ultimately tested during the calibration process. E, ν, tensile strength for the bolts were set to 210 GPa, 0.3, and 105 kN, respectively, per Mohamed et al.[41]

It is acknowledged that spacing of the rockbolt nodes may have some effect on its interaction with the blocks, particularly in cases where there are multiple blocks between nodes. In this case, the nodes were spaced at 0.05 m such that there was at least one node in each of the bolted blocks. Lastly, as UDEC scales various support parameters depending on the spacing in the out-of-plane direction,[70] this was set to 1 m and 2 m for the 1.2 m and 1.8 m bolts, respectively.

The Voronoi block contact parameters had the greatest degree of uncertainty associated with them and they were modified over a much wider range than the others. The greatest confidence was placed in the support and zone input parameters (meaning these were modified least from their initial values). c_{res}, $\sigma_{t,res}$ were assigned zero values, as only frictional forces can exist along fracture surfaces, while j_{kn}, j_{ks} were chosen to be large enough to so as to avoid the contacts affecting the overall modulus of the coal seam. In total, 9 model parameters were modified during the calibration process: c_{peak}, $\sigma_{t,peak}$, φ_{peak}, φ_{res}, peak cohesion of zones, residual friction angle of zones, critical plastic shear strain, S_{bond} and K_{bond}. Since the ranges of some of these parameters were constrained (bolt and zone parameters, specifically), the calibration process focused on adjustment of a limited number of parameters.

The contact parameters were calibrated by first varying them individually to understand their effect on the model response, followed by simultaneous changes to multiple parameters (considering the ones that had the greatest impact) until the field measured displacement and stress profiles could be reasonably reproduced. Contact tensile strength and residual friction angle were noted to have the largest influences on the model behavior.

Some erratic trends, similar to those reported in Sinha and Walton,[59] were also observed in the current study. In particular, it was found difficult to control the displacements and stresses by small systematic changes to the different input parameters; the behaviors, however, were consistent with expectation when large changes were introduced to the parameters. This issue will be discussed in context of actual model results. Secondly, when the zone strength parameters were made too strong, the rib displacements were found to decrease drastically. This occurred due to block movements contributing more towards the rib displacements and further highlights the need to introduce inelasticity in the Voronoi blocks, especially when the block size cannot be made very small.

Table 4 lists the calibrated set of model parameters. A high contact tensile strength was required for the contacts to prevent the blocks from buckling into the entry at low stress levels. Damage initiated first at the pillar corners through zone yield that eventually led to explicit fracturing along the block boundaries. If the damage was forced to initiate along block boundaries first, then the final model displacements were too large. This is illustrated in Fig. 5 in form of rib displacement contours after the development relaxation stage (i.e. before "zeroing" for comparison of the headgate loading displacements to the extensometer data) with inelastic (Fig. 5a) and elastic (Fig. 5b) blocks. As can be seen, when the blocks were elastic, the displacements with the same contact properties were more than 200% of those with inelastic blocks. It seems that it is important to allow finer-scale damage to initiate first via zone yield at the corners in order to prevent extensive fracturing along the rib. Although the initial zone strength is lower than the contact strength in the model with inelastic zones, due to point loading and wedging of blocks, damage ultimately progressed via explicit cracking rather than through zone failure along the rib (i.e. under low confinement conditions).

Table 4
Calibrated set of parameters. The zone properties were assigned to both the Voronoi section and the continuum section of the coal seam. Stiffness and strength properties for rockbolt grout are represented in terms of unit structural element length in UDEC, and hence the units are different than what is conventionally considered in rock engineering.

Zones - CWFS		Contacts		Rockbolt	
E (GPa)	3.0	c_{peak} (MPa)	13.9	Grout cohesive capacity (MN/m)	0.126
Peak cohesion (MPa)	8.4	c_{res} (MPa)	0	Stiffness of grout (MN/m/m)	1800
Residual cohesion (MPa)	0	φ_{peak} (°)	37	Modulus (GPa)	210
Peak friction angle (°)	0.0	φ_{res} (°)	27.5	Tensile strength (kN)	105
Residual friction angle (°)	55	σ_t (MPa)	12		
Tensile strength (MPa)	3	Normal stiffness (GPa/m/m)	80,000		
Critical plastic shear strain from peak to residual	0.035	Shear stiffness (GPa/m/m)	40,000		

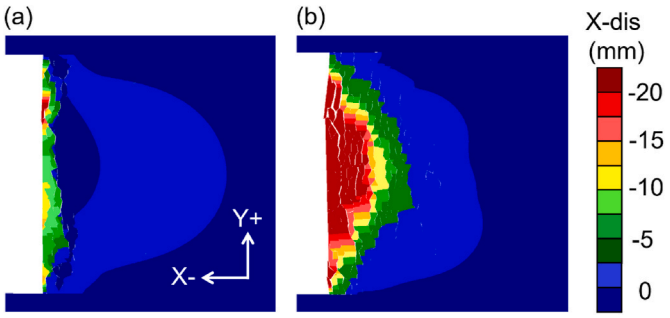

Fig. 5. Rib displacement contours after development relaxation with (a) Inelastic, and, (b) Elastic blocks. Note that these displacements are presented relative to the initial unexcavated condition rather than the post-development-relaxation datum used to compare model results to the extensometer data.

With respect to the CWFS parameters, the critical plastic shear strain and the peak cohesion had to be changed from 0.0081 to 7.1 MPa in Sinha and Walton[48] to 0.035 and 8.4 MPa. The critical plastic shear strain is a zone-size dependent parameter and must be increased with reduction in zone size to obtain similar behaviors.[72] The zones in Sinha and Walton[48] were cubic and 0.1 m long; the zones are much smaller in this study, and an increase in critical plastic shear strain is therefore justifiable. With respect to the change in peak cohesion, the increase can be explained on grounds that the overall strength of a rockmass, composed of intact rock blocks and bounded by explicit fracture pathways, is lower than the strength of the intact rock components. In other words, to achieve an equivalent rockmass strength to that represented by the continuum model of Sinha and Walton[48] when accounting for explicit fractures, the material strength within the Voronoi blocks needed to be increased.

3.2. Model results

Fig. 6 compares the rib displacement profile and stress profile as measured in the field with those from the calibrated BBM. The overall

shape of the displacement profile was well replicated by the BBM (Fig. 6a). From both the field data and the model results, it can be seen that the depth of significant fracturing lies in the range of 1–2 m from the rib surface, beyond which the behavior is nearly elastic. This explains why only the outer 4 m of the coal pillar was modeled using the elongated Voronoi blocks.

The measured change in vertical stress 4 m into the pillar (stress cell location in the field) was also well reproduced by the BBM (Fig. 6b). The continued increase in stress is likely related to both the advance of the longwall face (see Fig. 2a) as well as the fracturing of the outer skin pushing the stresses deeper into the pillar. Additionally, the sudden jump in displacement between the 4.5 MPa and 6 MPa stress datapoints could be replicated by the model, but the jump may occur slightly sooner in the model than in reality (it is difficult to assess definitively given the lack of multiple data points in this range and the variability in the data). It is at this stage when the depth of fractured contacts suddenly increased in the BBM from ~0.3 m to ~1.1 m.

During model calibration, the authors identified multiple parameter sets that exhibited slightly better agreement with the stress data but showed mismatch with respect to the rib displacement profile. Two such model results, termed as Alternate 1 and 2, are shown in Fig. 7. The only difference between the parameters of Alternate 1 and 2 and the calibrated model is that Alternate 1 and 2 had S_{bond} values of 125647.46 N/m and 125647.47 N/m while the calibrated model had a S_{bond} of 125620 N/m. As can be seen, the model behaviors were extremely sensitive to small parameter changes. Moreover, the increase in the S_{bond} necessarily did not lead to a delayed increase in displacements when the change was very small (the displacement jump in Alternate 1 occurred slightly later than in Alternate 2), but it did when the change was larger (Alternate 1 and 2 had both had delayed displacement increases in comparison to the calibrated model). Since the calibrated model showed reasonable fit to both the displacement profile and the stress data, the authors decided to use this parameter set for the rest of the study.

The evolution of fractured contacts and yielded zones in the calibrated model as a function of headgate loading is shown in Fig. 8. The depth of fracturing increased from Stage 10 to Stage 15 and then remained almost constant up to Stage 33. The rapid displacement increase shown in Fig. 6b occurred at Stage 15 in the model. Based on a comparison of Stage 10 and Stage 15 in Fig. 8, one can recognize how the depth of fractured contacts has almost tripled. This also occurred in the field when the face crossed the 58 m outby location and then remained constant until the end of the monitoring period (Fig. 2b). Interestingly, this increase in depth of fracturing could not be replicated by both Sinha and Walton[48] and Mohamed et al.[41] using FLAC^{3D} models. We believe that it was possible to reproduce this behavior in BBM because of its ability to model discontinuous and localized damage processes efficiently.

The lower boundary of the red contour, i.e. $\varepsilon_{ps} > 0.0035$, increased with increasing vertical stresses. At an early stage (Stage 10), there was some yield at the corners. As loading continued, the extent of the yielded regions increased and formed a V-shaped region just at the edge of the fractured contacts. Such a V-shaped shear zone appears to be characteristic of stress-driven brittle failure processes, and has previously been observed in model results by Carter et al.,[73] Edelbro,[74] Sinha and Walton[49,59] and Renani and Martin[75]. Within the region of explicit fracturing, the number of yielded zones was minimal. This means that failure near the pillar boundary indeed occurred via contact failure (highly dilatant) while it occurred via zone yield for regions deeper within the pillar (minimal dilation). The fracturing and zone yielding also locally reduced the load carrying capacity of the coal rib and pushed the excess stress deeper into the pillar; the stress distribution in the rib at Stage 10 and 30 can be found in the Supplementary Materials. Such a boundary-relaxation-core-loading phenomenon was observed by Wagner[76] in the field and is also evident from the stress data in Esterhuizen et al.[77] Lastly, it can be noted how the failure of the joint elements bounding the coal seam also propagated deeper, allowing the coal layer to slip and accommodate the deformations due to fracturing and yielding of the coal pillar.

Fig. 9 shows the axial load in the upper and lower rib bolt for the calibrated model. At early stages of loading, some local peaks can be identified in the upper rib bolt that are associated with fracture development in the model (Fig. 9a). As soon as the depth of fracturing increased at Stage 15, the bolt attained yield strength for ~50% of its length, and there was also some failure of the bolt-grout interface. With continued loading, the bolt elements closest to the rib also attained yield strength and the length of the yielded section increased slightly. The decay in the bolt axial load to the right of the yielded region implies that it is still transferring some amount of the load into the coal and providing reinforcement to the fractured rib.

In the lower bolt, a slightly different trend was observed (Fig. 9b). It began to yield at an early stage of loading (Stage 10) at a specific location that corresponded to a local fracture in the model. As the headgate loading continued, a steady decline was noted in the peak load level. A closer look at the model results revealed a complete failure of the bolt-grout interface at Stage 15. Consequently, as the ribs continued to deform laterally, the entire rib bolt slipped and this resulted in a loss of axial load. To further understand this trend, it is useful to revisit the structural representation of bolts in UDEC. The interaction between the rockbolt nodes and zone vertices (also called gridpoints) is simulated by a spring/slider system in UDEC.[70] When the local differential movement between a node and its neighboring gridpoints increases, the load in the grout increases as well as a linear function of the grout stiffness, until the

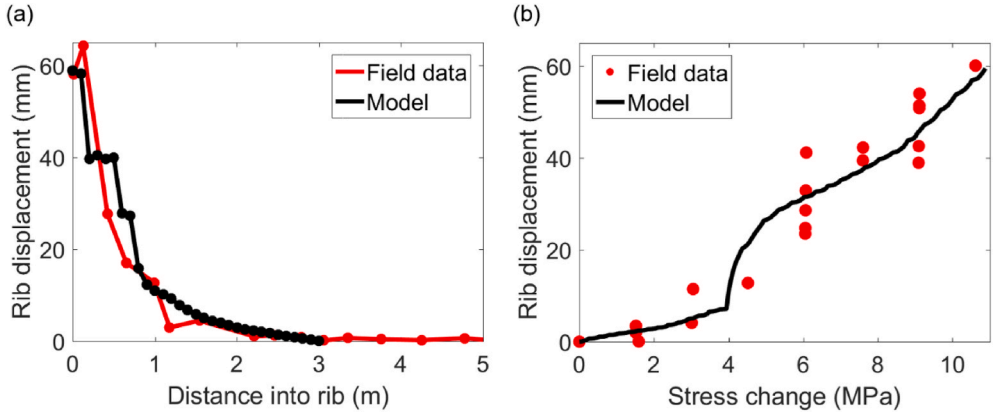

Fig. 6. (a) Rib displacement profile, and, (b) Stress change versus rib displacement as measured in field and those in the calibrated model. The displacements are presented with respect to the displacements measured when the longwall face was 52 m inby in the field (initiation of headgate loading at a longwall face position of −52 m).

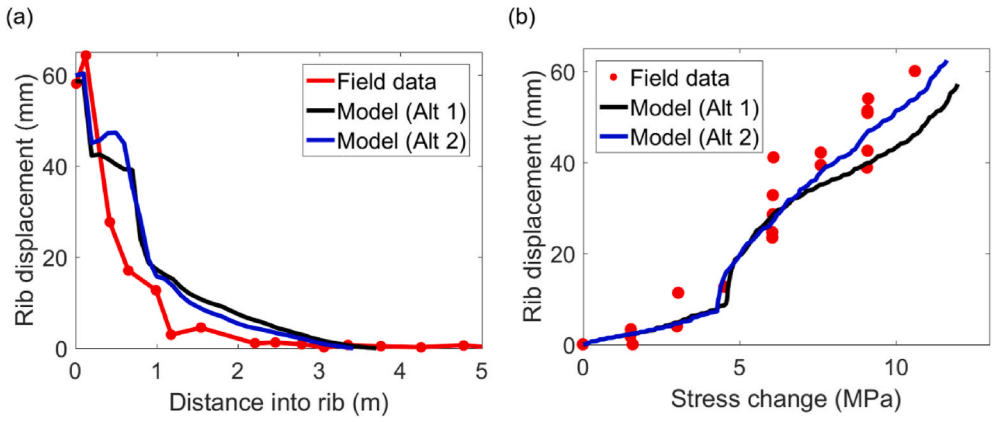

Fig. 7. (a) Rib displacement profiles, and, (b) Stress change versus rib displacement as measured in field and those in two alternate models. The displacements are presented with respect to the displacements measured when the longwall face was 52 m inby in the field (initiation of headgate loading at a longwall face position of −52 m).

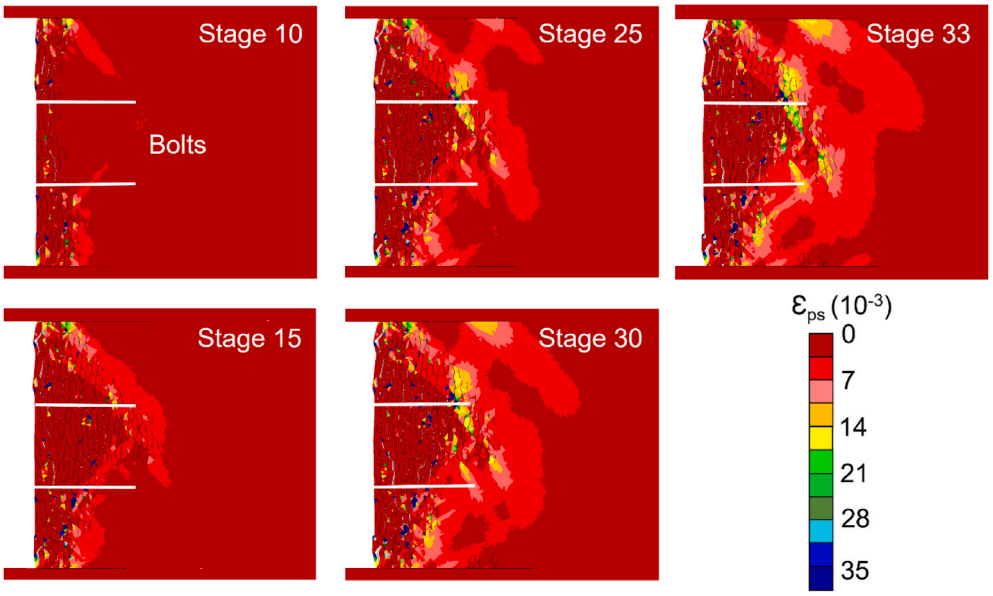

Fig. 8. Fracture pattern and plastic shear strain contour for 5 different stages of headgate loading. Stage "1" corresponds to the model state prior to headgate loading (i.e. after development entry relaxation), and Stage "33" corresponds to the model state after 33 stages of headgate load increase.

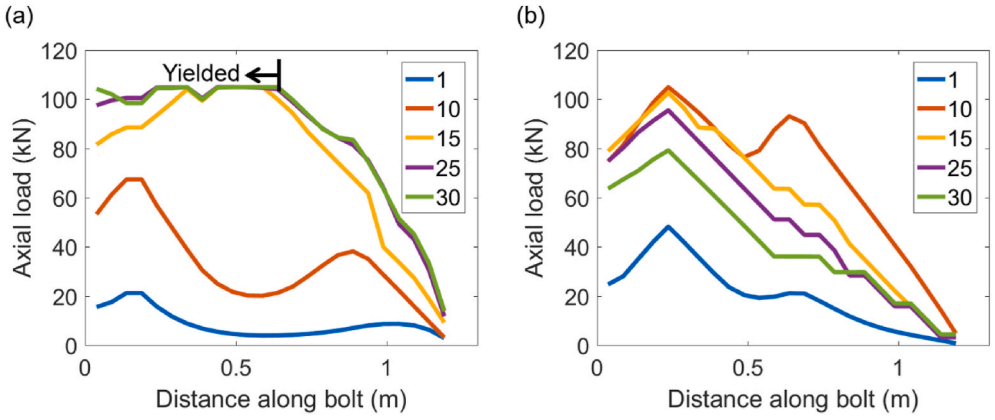

Fig. 9. Axial forces in the (a) top, and, (b) bottom rib bolt as a function of stage number.

peak strength is attained. Upon attaining the peak grout strength, the rockbolt slides with additional deformation in the rock, providing only a constant resistive force (equivalent to the grout strength) to the zone gridpoints. With that in mind, the axial load in the bolts is calculated with respect to the strain between neighboring nodes of the rockbolt. It seems that at later stages of loading, when the rib started to buckle, the entire rockbolt moved with the ground, reducing the differential movements between neighboring nodes and hence the associated axial loads. At all stages of simulation, the displacement of the outermost node in the lower bolt was found to be greater than in the upper bolt (referring to Fig. 10b for one such stage; the rock displacement provides an approximation of the nodal displacement) and this explains why such a behavior was not observed in the upper rib bolt.

The bolt load profile shown in Fig. 9a is rather different from Sinha and Walton[48] due to the fact that Sinha and Walton[48] did not consider any face plates. Accordingly, for all rock-grout interfaces that failed, the axial loads were very low and, in some cases, almost zero. In this study, face plates were simulated using elastic beam elements and the last nodes of the rockbolts were merged with the central nodes of the face-plates. Because of this indestructible connection, failed sections of the rockbolts still continued to carry load up to their yield strength.[78] Although the model shows that the bolts are providing some reinforcement, it seems that they are approaching their ultimate capacities and with further loading (e.g. continued first abutment or second abutment loading), it is possible that their reinforcement capability will be completely lost. This is supported by the description of the tailgate intersection (location where the longwall face intersects the tailgate entries) in Colwell[14] for the adjacent panel: "The effects of second front abutment loading associated with the current longwall were evident to a distance of approximately 30 m outby of the face. Rib spall within this zone of 0.5 m–1 m was observed on the block side rib …". When 0.5–1 m of the rib was reported to have visibly spalled, it is likely that rockbolts, which were only 1.2 m long, were ineffective by this point.

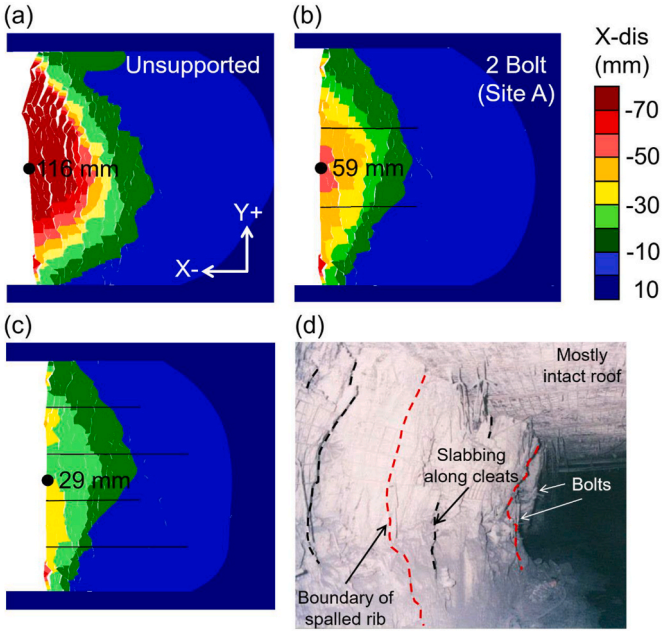

Fig. 10. Rib displacement contours for (a) unsupported condition, (b) 2 bolt condition (calibrated) and (c) 4 bolt condition. The displacements are presented with respect to the displacements measured when the longwall face was 52 m inby in the field (initiation of headgate loading at a longwall face position of −52 m). (d) A picture from a different location in the panel long after the first passage of the longwall face is shown on the bottom right (after[14]).

4. Effect of rib supports

With the reliability of the BBM established, the next task was to investigate the effect of alternate support patterns on the model response. To that end, the calibrated model was re-run with no support and with 4 bolts. Fig. 10(a–c) shows the horizontal displacement contour for the unsupported, 2 bolt (calibrated to Site A) and 4 bolt (Site B) models. The displacement at the mid-height of the pillar at the periphery and the state of rib at a different location in the same panel is also shown in Fig. 10d. Comparing with the photograph from the field (taken long after the first passage of the longwall face), a similarity can be noted in the shape of the spalled region and the −40 mm displacement contour in the model. In particular, the lower "limb" of the damaged region is steeper than the upper portion in both the model and the photograph. Unlike in the photograph, the damaged region in the BBM did not separate from the pillar and collapse, and this is attributed to two factors: (1) the photographed rib was subjected to further abutment loading beyond that considered at the instrumented site; (2) the instrumented locations were noted to be anomalously more stable than other regions in the panel, such as the photographed rib[14]: "Further communication with colliery personnel indicated that there was no significant increase in spall over and above that observed on 18/11/02, which is also supported by the extensometry data. The colliery commented that this was not typical and that normal rib behaviour at significant distances inbye of the face is better illustrated by Plate 2". 18/11/02 corresponds to 416 m outby face location, and Plate 2 is the photograph shown in Fig. 10d. Note the columnar shape of slabs along the rib, which is consistent with the use of elongated blocks in this study. Also, the condition of the roof in the picture is consistent with the use of an elastic constitutive model for the roof and floor in the model.

When the two rockbolts were removed from the model, a remarkable increase in displacement from 59 mm to 116 mm (or 97% increase) was observed. Comparing with the continuum FLAC^{3D} model of Sinha and Walton,[48] only a nominal 5–6 mm increase was noted when the supports were omitted. For the 4 bolt model, the rib displacement at the periphery was 29 mm (Fig. 10c). This corresponds to a 50% drop in displacements with respect to the 2 bolt model and is only 6 mm more than what was measured in the field.[12,14] It is interesting to note here that the match to Site B displacement was not a focus of model calibration, but an emergent behavior of the BBM when the two extra bolts were added (same properties as those in Table 4). The similarity between the model-predicted displacements and field measurements confirms that BBMs can reproduce ground behaviors under varying support conditions.

While there are many possible explanations for the 6 mm discrepancy between the 23 mm rib displacement measured at Site B and the 29 mm rib displacement in the 4 bolt model, we believe it may relate to the different degrees of rib damage at Site A and B at the start of the headgate loading stage (Stage 1). In the field, almost zero rib displacement was measured at Site B while ~12 mm was measured at Site A when the longwall face was 52 m inby of Site A.[14] What this means is that after the extensometers were installed at both sites, there was some movement at Site A before the first set of readings was taken (−52 m longwall face position). Due to the presence of additional support, any such movement that would have occurred at Site B was suppressed, and hence no deformation was recorded by the extensometer. As the BBM was initially calibrated to Site A and then used to simulate Site B, a ~12 mm displacement was present in both models following the development relaxation stage (before zeroing the displacements in the model; see Fig. 5a). The difference in the rib conditions at the start of the headgate loading stage was therefore ignored in the BBM, and this might have led to the 6 mm mismatch between the model and the field data.

To better understand how the progressive damage development was affected by the incorporation of 2 additional bolts, vertical stress changes at a point 4 m into the pillar (stress measurement location) were plotted as a function of the rib displacement and are shown in Fig. 11. An

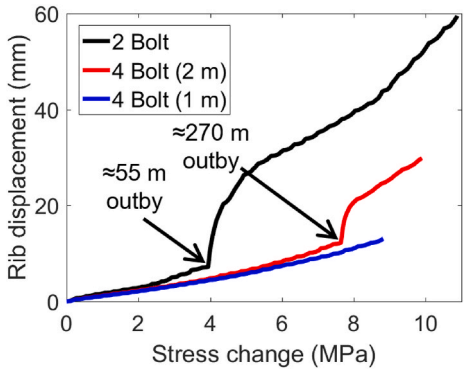

Fig. 11. Rip displacement versus stress change for the 2 bolt model (calibrated) and the 4 bolt models. The displacements are presented with respect to the displacements measured when the longwall face was 52 m inby in the field (initiation of headgate loading at a longwall face position of −52 m).

additional model was run with an out-of-plane spacing of 1 m for the 1.8 m bolts and is also shown in Fig. 11; this alternative case corresponds to a higher support density than what was installed at Site B. For purposes of comparison, the plot for the calibrated 2 bolt model is also shown (same as in Fig. 6b). As can be seen, the point of the sudden displacement increase was delayed by ~4 MPa in the 4 bolt (2 m) model. It should also be noted that the magnitude of increase is significantly lower in the 4 bolt (2 m) model, implying that the bolts not only reduced the depth of significant fracturing (Fig. 10c) but also suppressed the dilatancy within the stress-fractured region.

The sudden jump in the 4 bolt (2 m) model occurred at loading Stage 26, which corresponds to a ~270 m outby longwall face location for Site A. The equivalent longwall face location was determined by identifying the stress magnitude at loading Stage 26 in the calibrated 2 bolt model and then relating it to Fig. 2a (recall that the stress data in Fig. 2a is for Site A). According to the extensometer data of Colwell,[14] the sudden increase in displacement at Site B occurred when the face was about 440 m outby of Site A (Stage 29). The slightly premature displacement increase at Stage 26 in the model (Fig. 11) is also consistent with the potential effect of the different rib conditions that existed at the start of headgate loading. If less contacts had failed after development relaxation (Stage 1) for the 4 bolt model, then it might have been possible to further delay the jump to occur closer to a stress corresponding to 440 m outby of site A. Lastly, it can be seen in Fig. 11 that when the out-of-plane spacing for the 1.8 m bolts was reduced to 1 m, the jump did not occur at all and the displacements were further suppressed. Indeed, the higher support density layout is effective in preventing the generation and separation of stress-induced spalling fractures.

Further analysis of the support effect was conducted via calculation of bulking factors for the unsupported, 2 bolt and 4 bolt (2 m out-of-plane spacing) models. Bulking factor is defined as the percentage of volume increase within the yielded zone from an undamaged state.[79,80] Since UDEC is a 2D software, it is the area generated by the stress-fractures rather than the volume which was considered during the calculation. For determination of bulking factor (BF), the following equation from Kaiser et al.[56] was used:

$$BF = \frac{u_w - u_{d_f}}{d_f} \tag{2}$$

where, u_w is the displacement at the rib, u_{d_f} is the displacement at the depth of failure, and, d_f is the thickness of the fractured rock. To determine the three parameters, lateral displacements of all gridpoints along 5 horizontal lines were extracted from the model. These lines were extended to 1.5 m into the rib and were spaced at 0.5 m vertically (Fig. 12a inset). Fig. 12a shows the lateral displacements for the 2 bolt model. The numbers in the legend represent the location of the horizontal lines from the base of the coal seam. Although it would have been simpler to select just one section along the mid-height of the pillar and compute the BF, it would not be representative of the entire pillar because of the non-uniform shape of the damaged zone (see Fig. 10a–c). In particular, fracturing was greatest at the center and diminished along the edges. It was therefore decided to compute the bulking factor separately along the 5 horizontal lines.

d_f was manually identified as the point where the perturbations in the lateral displacements diminished and the curve became smooth. These points are marked by the black solid circles in Fig. 12a. Once the d_f was identified, it was rather straightforward to determine u_w and u_{d_f} from Fig. 12a as the displacements at the rib surface and at d_f, respectively. As the horizontal axis in Fig. 12a corresponds to the undeformed location of the gridpoints, the comparison to an undamaged state is implicitly accounted for in the BF equation. Additionally, when displacements across the fractured region are subtracted (numerator of Eq. (2)), the explicit contact damage and the inelastic yield in the block zones are accounted for (although the latter is minimal at the pillar periphery).

The computed BF for all three models and their mean values are shown in Fig. 12b. As expected, the BF dropped in an exponential fashion with increase in support density, which is consistent with the empirical findings of Kaiser et al.[56] A direct (quantitative) comparison against the empirical data of Kaiser et al.[56] is not appropriate in this case

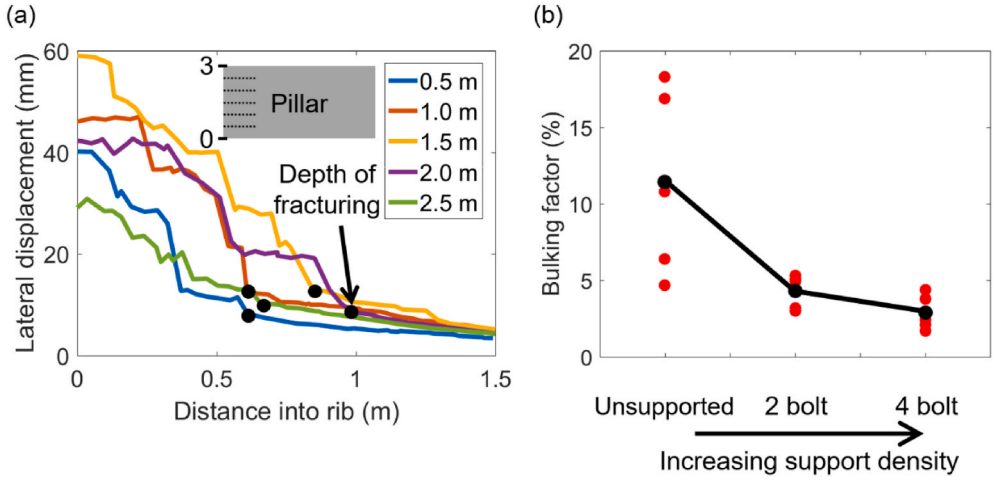

Fig. 12. (a) Methodology followed for determination of the edge of the fractured region, and, (b) Bulking factors along horizontal lines located at different heights in the coal pillar for the unsupported, 2 bolt and 4 bolt BBM.

because that data is based on observations in hard rocks (like granite). However, since coal is brittle in nature and also undergoes spalling, the trend is at least expected to be similar.

The decline in the marginal benefit of added support with an increase in support density can be explained using the conceptual framework for ground-support interaction presented by Sinha and Walton.[12] Specifically, one can split the ground-support interaction curve, plotted in support effect-support density space, into three segments: (1) Inadequate support segment – Support density is not adequate and it breaks leading to minimal effect on ground behavior; (2) Maximum gain segment – Increase in support density has the maximum marginal "value added" in this region; and (3) Overdesigned segment – an excessive amount of support has been added to the system, and the effect of any further support on the ground is limited. In this final segment, the ground has already been sufficiently reinforced such that it behaves as a continuum. With this framework in mind, it seems that the 2 bolt layout is in the Maximum gain segment and it manages to suppress the dilation of fractures efficiently, while the 4 bolt layout is near the boundary between the Overdesigned and Maximum gain segments. Note this classification only holds for the specific loading condition tested in this study. With additional mining-induced stresses (e.g. second abutment loads) coming onto the pillar, the rib can fail even with the 4 bolt layout (as previously noted), and at that point, the layout could be considered as 'inadequate' or 'under-designed'.

5. Effect of block shape

The modeling of fracturing in anisotropic rock depends heavily on the shape anisotropy of the constituent blocks. For coal, the block aspect ratio was established through simulated small-scale compression tests in this study. To further understand how block shape might be controlling the fracturing and yield in the models, as well as its mechanical interaction with support, a separate back-analysis was conducted using isotropic Voronoi blocks. For this purpose, the model geometry described in Section 2.1 was employed and the elongated blocks were replaced with regular isotropic blocks of the same height.

The rationale behind selecting the same height was twofold: the number of blocks along the seam height should be kept consistent with that in the elongated block model, and the same zone size should be used as in the elongated block model; this eliminates the need to re-calibrate the zone inelastic parameters. Additionally, the support parameters listed in Table 4 could also be used, meaning that the only modifications required were in the contact parameters (this is natural, since the contact geometry was the only other change made in the model).

A manual back-analysis was subsequently conducted using the isotropic Voronoi block geometry, and it was possible to determine a set of contact properties that resulted in a reasonable match with the field extensometer and stress measurements. Table 5 lists the calibrated contact parameters for this model, and Fig. 13 compares the model results to the field measurements at Site A. A lower contact tensile strength was required, as the propensity of the blocks to separate laterally was lower in this case. As can be seen, the model was able to match the field extensometer measurements very well (Fig. 13a) and this agreement is marginally superior to that obtained in the elongated block model case. The trend of the stress data (Fig. 13b) was also well reproduced for the entire range of headgate loading considered.

Figs. 14 and 15b shows the horizontal displacement contours after the entry loading stage and the headgate loading stage, respectively. The displacement at the pillar mid-height after the development relaxation stage is similar to that in Fig. 5a; the fracturing, however, is much more localized in the latter case. For the 2 bolt model, the depth of fracturing and displacement at pillar mid-height are also similar (compare Figs. 10b, 13a and 6a).

The calibrated model was subsequently re-run without supports (unsupported) and with 4 bolts, considering out-of-plane spacings of 1 m and 2 m for the longer bolts. The displacement versus vertical stress results for these models are shown in Fig. 13b. As expected, the unsupported model underwent a rapid increase in displacement at early stages of headgate loading but stabilized at around a stress of 2 MPa. Following this point, the rate of displacement increase was similar to that of the 2 bolt model. In comparison to the elongated model, the displacement at the pillar mid-height is much lower following the headgate loading phase. This is explained by the breakage and separation of a large portion of the rib in the upper half of the pillar (Fig. 15a); the lateral displacement of the separated part is 162 mm while at the mid-height, it is only 72 mm. Such a behavior was not observed in the elongated block model, as the blocks buckled along the vertical failure planes in that case.

Both the 4 bolt models exhibited delayed displacement increases in comparison to the 2 bolt model. At late stages of headgate loading, the displacements started to rise, first in the out-of-plane 2 m model followed by the 1 m model (out-of-plane 1 m layout corresponds to greater support density than 2 m). This increase is attributed to a combination of both grout failure and bolt breakage. Overall, the addition of two bolts seems to restrict rib cracking and dilation (Fig. 15c), but eventually the movements exceeded the reinforcement capacity of the rock support.

The difference in the behaviors observed in the elongated and isotropic block models can be simplistically explained as follows: in the elongated block models, there is a buckling tendency in the lateral direction, and incorporation of supports tend to bind/tie these layers together. From Euler's buckling theory,[81] it is known that the critical bulking load is related to the area moment of inertia, which for a beam is proportional to $(\text{width})^3$. If rockbolts are capable of effectively binding the layers together, then it would raise the critical bulking load dramatically. This explains why drastic changes in rib behavior (Fig. 12b) were obtained in the elongated block models with inclusion of additional bolts. This is of course a simplification of the actual ground behavior, which involves fracturing between the layers and differential buckling, but the explanation serves as a useful conceptual model as a first order approximation. Note that buckling is a well-documented mode of failure associated with coal ribs.[28,29,82]

In the regular Voronoi models, the blocks do not exhibit a pure buckling tendency, but rather also incorporate a notable degree of shearing in their movement. This is because these blocks are isotropic in shape and thus have equal pathways for failure in the vertical and horizontal direction. When the models were examined more closely, it was found that the fracture openings in the elongated block model were more uniformly distributed along multiple contacts but were concentrated along a limited number of block edges in the regular model; this is logical, as there are a smaller number of sub-vertical fracture elements in the isotropic Voronoi model being used to create the same displacement profile as in the anisotropic model. Due to the aforementioned shearing mechanism and the high strain concentrations, some of the rockbolts were also found to rupture under the headgate loading condition in the isotropic Voronoi models. On the contrary, loading in the rockbolts in the elongated block models was mostly in the axial direction, and consequently almost no bolt elements ruptured. From this discussion, it is understandable that the isotropic blocks do not reproduce the same rock damage mechanisms as are reproduced by the elongated blocks. An additional finding is that just because a BBM model is well calibrated (e.

Table 5
Calibrated set of contact parameters for regular Voronoi model.

Parameter	c_{peak} (MPa)	c_{res} (MPa)	φ_{peak} (°)	φ_{res} (°)	σ_t (MPa)	Normal stiffness (GPa/m/m)	Shear stiffness (GPa/m/m)
Value	16.5	0	41	27.5	8	80,000	40,000

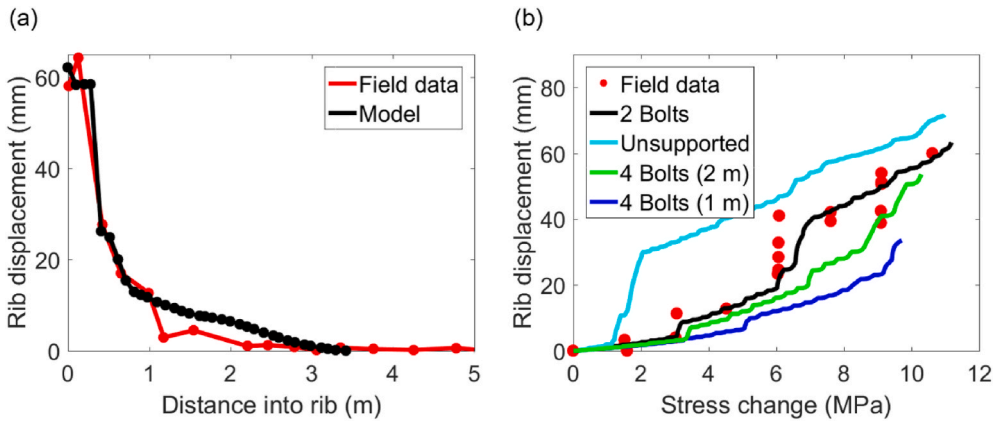

Fig. 13. (a) Rib displacement profiles, and, (b) Stress change versus rib displacement as measured in field and those in the different models. The displacements are presented with respect to the displacements measured when the longwall face was 52 m inby in the field (initiation of headgate loading at a longwall face position of −52 m).

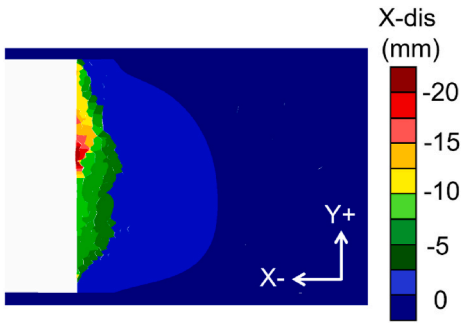

Fig. 14. Rib displacement contours after development relaxation stage. Note that these displacements are presented relative to the initial unexcavated condition rather than the post-development-relaxation datum used to compare model results to the extensometer data.

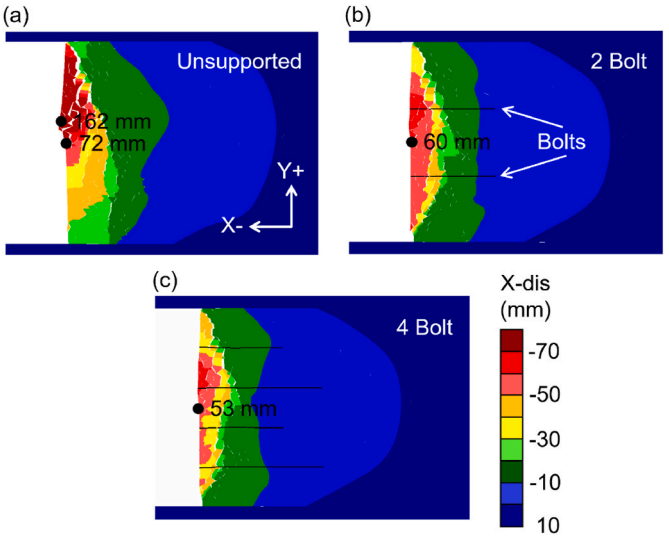

Fig. 15. Rib displacement contours after (a) unsupported condition, (b) 2 bolt condition and (c) 4 bolt condition. The displacements are presented with respect to the displacements measured when the longwall face was 52 m inby in the field (initiation of headgate loading at a longwall face position of −52 m).

g. the 2 bolt case), it cannot be expected to produce reasonable forward predictions (e.g. the 4 bolt case) if the representation of ground behavior (in this case, the anisotropic buckling) is not correct.

6. Implications for rock engineering

The present study has demonstrated the ability of the elongated BBM approach to realistically reproduce cleat-induced anisotropy of coal mass as well as the influence of rockbolt reinforcement on ground behavior. These findings have some important design implications, especially in the domain of mining engineering.

As previously stated, design of coal mine rib supports still continue to be based on site-specific experience in the United States. The elongated BBM approach has the potential to aid in this design process through development of simple support charts. A schematic is presented in Fig. 16, where the Y axis is some measure of support density and the X axis represents the rib integrity. Support density could be related to the shear strength of rockbolt, length of rockbolt and spacing along and across the roadway, while rib integrity could consider variables like coal strength, bedding frequency strength, orientation of cleat planes with respect to roadway direction, presence of stone bands, mining depth, etc.[87] A wide suite of models considering various combinations of the

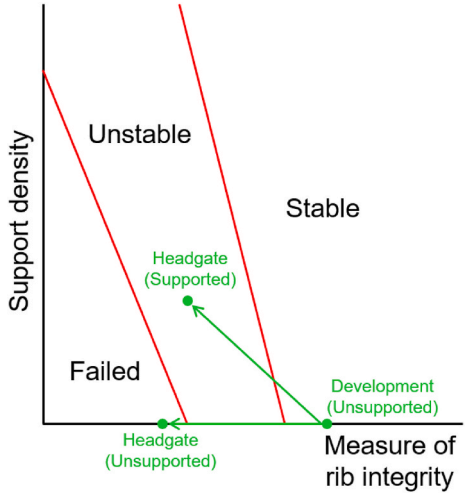

Fig. 16. Schematic of a hypothetical design chart that could be developed using the elongated BBM approach; points shown on the chart illustrate a hypothetical scenario where changes in rib stability through the transition from development loading to headgate loading conditions with and without support is assessed.

aforementioned properties and loading conditions (e.g. development, headgate) could be run to demarcate between stable, unstable and failed rib conditions, as shown in Fig. 16. With such charts available, a mine would be able to select a support density that would be appropriate for the geo-mining and loading conditions that exist at a given site.

A major advantage of elongated BBMs with respect to the proposed design approach is that the effect of different rock support types and patterns and the relative orientation of cleat planes can all be explicitly considered within these models. In fact, for studying the effect of cleat orientation, only the direction of elongation has to be modified, and this can now be conveniently controlled using the 'angle' option in the UDEC 7.0 Voronoi generator. Needless to say, such is difficult and often impossible when using a continuum model like FLAC.[12] Ubiquitous joints could be used in a continuum model to simulate strength anisotropy,[53–55,87] but it remains to be established how well this approach can replicate the ground-support interaction mechanism.[88]

The BBM approach also has the potential to improve our understanding of the interaction between rib damage and roof response. In the current study, the roof has been simulated as an elastic material, but for other geological conditions, it is possible to represent the roof using DFNs (e.g. Ref. 89) and/or an inelastic constitutive model. In such a case, the presence or absence of rib support would control the extent of stress-arching and displacements in the roof based on the influence of support on the rib's load-bearing capacity. With all this in mind, it is apparent how the findings of the current study represent a critical step towards potential applications of BBMs for various mining scenarios.

7. Conclusions

In this study, the Bonded Block Modeling approach was used to simulate the rib damage process in a longwall chain pillar located in West Cliff mine (Australia). The anisotropy of coal mass was represented using elongated Voronoi blocks. At the West Cliff mine, Colwell[14] installed extensometers and stress cells in two adjacent chain pillars that had different rib support densities and collected data as the longwall face approached and passed the instrumented pillars. The field data corresponding to the chain pillar with lower support density was specifically utilized for constraining the BBM input parameters. The model had the same rockbolt layout as was present at the site. After calibration, the model was able to replicate the rib displacement profile, stress changes as a function of longwall face location, and the depth of fracturing. The match against multiple field-measured attributes provided confidence in the back-analyzed BBM parameters.

The model was subsequently re-run without any support and with extra support to mimic the support condition at the adjacent chain pillar in the West Cliff mine. In absence of any support, the model predicted very high displacements (a ~97% increase) - much larger than what was obtained in previous continuum models of the same site. By incorporating the appropriate amount of additional support corresponding to the Site B pillar, model displacements within 6 mm of those recorded at this pillar were obtained. These results indicate that the elongated Voronoi block approach is not only capable of reproducing the rib damage phenomena but also the ground-support interaction mechanism, and therefore has the potential to be used in the development of a support design tool. Such tools could be simple design charts indicating the required level of support for a given mining depth or for different stages of mining, which could be constructed by testing various support patterns or loading conditions in similar site-specific BBMs. Design charts would ultimately help mines optimize their support designs without having to develop and calibrate BBMs themselves.

Finally, to understand the influence of block shape on damage development in the pillar models, a model with isotropic Voronoi blocks instead of elongated blocks was calibrated. Ultimately, it was found that this representation cannot reproduce the ground-support interaction mechanism accurately, which is ultimately related to the inability of isotropic blocks to properly simulate the behavior of anisotropic ground. In particular, the elongated block models showed a buckling tendency, and rockbolt installation increased the width of material undergoing buckling, thereby causing significant changes in the model results. In the isotropic Voronoi model, the buckling propensity was lower, and a greater degree of shearing was observed along the block contacts.

Declaration of competing interest

The authors declare that they have no known competing financial interests or personal relationships that could have appeared to influence the work reported in this paper.

Acknowledgement

The research conducted for this study was funded by the National Institute for Occupational Safety and Health (NIOSH) under Grant Number 200-2016-90154. The authors would like to extend their gratitude for the financial support. Special thanks to Dr. Mark Larson and Dr. Bo-Hyun Kim for reviewing this manuscript prior to submission and providing valuable suggestions. The modeling effort for this study was conducted using educational licenses of UDEC provided by Itasca Consulting, Ltd. The authors appreciate Itasca's support in this capacity.

Appendix A. Supplementary data

Supplementary data to this article can be found online at https://doi.org/10.1016/j.ijrmms.2021.104965.

References

1 Lan H, Martin CD, Hu B. Effect of heterogeneity of brittle rock on micromechanical extensile behavior during compression loading. *J Geophys Res: Solid Earth*. 2010;115 (B1).
2 Bahrani N, Kaiser PK, Valley B. Distinct element method simulation of an analogue for a highly interlocked, non-persistently jointed rockmass. *Int J Rock Mech Min Sci*. 2014;71:117–130.
3 Bewick RP, Kaiser PK, Bawden WF. DEM simulation of direct shear: 2. Grain boundary and mineral grain strength component influence on shear rupture. *Rock Mech Rock Eng*. 2014;47(5):1673–1692.
4 Abdelaziz A, Zhao Q, Grasselli G. Grain based modelling of rocks using the combined finite-discrete element method. *Comput Geotech*. 2018;103:73–81.
5 Sinha S, Shirole D, Walton G. Investigation of the micromechanical damage process in a granitic rock using an inelastic Bonded Block Model (BBM). *J Geophys Res: Solid Earth*. 2020:124.
6 Coggan J, Gao F, Stead D, Elmo D. Numerical modelling of the effects of weak immediate roof lithology on coal mine roadway stability. *Int J Coal Geol*. 2012;90: 100–109.
7 Lan H, Martin CD, Andersson JC. Evolution of in situ rock mass damage induced by mechanical–thermal loading. *Rock Mech Rock Eng*. 2013;46(1):153–168.
8 Gao F, Stead D. The application of a modified Voronoi logic to brittle fracture modelling at the laboratory and field scale. *Int J Rock Mech Min Sci*. 2014;68:1–14.
9 Bai Q, Tu S, Zhang C, Zhu D. Discrete element modeling of progressive failure of wide coal roadway from water-rich roofs. *Int J Coal Geol*. 2016;167:215–229.
10 Shen B. Coal mine roadway stability in soft rocks: a case study. *Rock Mech Rock Eng*. 2014;47:2225–2238.
11 Bahrani N, Hadjigeorgiou J. Influence of stope excavation of drift convergence and support behavior: insights from 3D continuum and discontinuum models. *Rock Mech Rock Eng*. 2018;51(8):2395–2413.
12 Sinha S, Walton G. Understanding continuum and discontinuum models of rock-support interaction for excavations undergoing stress-induced spalling. *Int J Rock Mech Min Sci*. 2019;123:104089.
13 Larson MK, Dunford JP. *Two case studies of the performance of rib supports*. Golden Colorado, USA. *Proceedings of 15th Conference on Ground Control in Mining*. 1996: 527–542.
14 Colwell MG. *A Study of the Mechanics of Coal Mine Rib Deformation and Rib Support as a Basis for Engineering Design*. Australia: Ph.D. thesis, University of Queensland; 2006.
15 Mohamed KM, Murphy MM, Lawson HE, Klemetti T. Analysis of the current rib support practices and techniques in US coal mines. *International Journal of Mining Sciences and Technology*. 2016;26(1):77–87.
16 Wanne T, Johansson E, Saanio DP. reportÄspö Pillar Stability Experiment Final Coupled 3D Thermo-Mechanical Modeling and Preliminary Particle-Mechanical Modeling. SKB, Report R-04-03 2004.
17 Cai M, Kaiser PK, Morioka H, et al. FLAC/PFC coupled numerical simulation of AE in large-scale underground excavations. *Int J Rock Mech Min Sci*. 2007;44(4):550–564.
18 Kias MEC, Ozbay U. *Modeling unstable failure of coal pillars in underground mining using the discrete element method*. San Francisco, US. *Proceedings of 47th US Rock Mechanics/ Geomechanics Symposium*. 2013. Paper No. 174.

19 Elmo D, Stead D. An integrated numerical modeling - discrete fracture network approach applied to the characterization of rock mass strength of naturally fractured pillars. *Rock Mech Rock Eng*. 2010;43(1):3–19.
20 Li X, Kim E, Walton G. A study of rock pillar behaviors in laboratory and in-situ scales using combined finite-discrete element method models. *Int J Rock Mech Min Sci*. 2019;118:21–32.
21 Vazaios I, Diederichs MS, Vlachopoulos N. Assessment of strain bursting in deep tunnelling by using the finite-discrete element method. *Journal of Rock Mechanics and Geotechnical Engineering*. 2019;11(1):12–37.
22 Gao F, Stead D, Kang H. Numerical investigation of the scale effect and anisotropy in the strength and deformability of coal. *Int J Coal Geol*. 2014;136:25–37.
23 Christianson M, Board M, Rigby D. *UDEC simulation of triaxial testing of lithophysal tuff. Proceedings of 41st U.S. Rock Mechanics/Geomechanics Symposium*. Golden: Colorado; 2006. Paper No. 968.
24 Preston RP, Stead D, McIntire H, Roberts DP. *Quantifying the effects of adverse geology on pillar strength through numerical modeling. Proceedings of 47th US Rock Mechanics/Geomechanics Symposium*. San Francisco, California: US; 2013. Paper No. 478.
25 Muaka JJ, Duma S, Mushangwe P, et al. *Modelling hard rock jointed pillars using a distinct element and discrete fracture network approach considering the effect of a clay-filled shear structure*. Perth, Australia. *Proceedings of the 8th International Conference on Deep and High Stress Mining*. 2017:311–328.
26 Kim B, Walton G, Larson MK, Berry S. Experimental study of the confinement-dependent characteristics of a Utah coal considering the anisotropy of cleats. *Int J Rock Mech Min Sci*. 2018;105:182–191.
27 Song H, Jiang Y, Elsworth D, Zhao Y, Wang J, Liu B. Scale effects and strength anisotropy in coal. *Int J Coal Geol*. 2018;195:37–46.
28 Smith WC. *Rib Stability: Practical Considerations to Optimize Rib Design*. US Department of the Interior, Bureau of Mines; 1992.
29 Jones T, Mohamed K, Klemetti T. *Investigating the contributing factors to rib fatalities through historical analysis. Proceedings of the 33rd International Conference on Ground Control in Mining*. WV: Morgantown; 2014:113–122.
30 Vardar O, Zhang C, Canbulat I, Hebblewhite B. Numerical modelling of strength and energy release characteristics of pillar-scale coal mass. *Journal of Rock Mechanics and Geotechnical Engineering*. 2019;11(5):935–943.
31 Kang HP, Lin J, Fan MJ. Investigation on support pattern of a coal mine roadway within soft rocks—a case study. *Int J Coal Geol*. 2015;140:31–40.
32 Chen M, Yang SQ, Zhang YC, Zang CW. Analysis of the failure mechanism and support technology for the Dongtan deep coal roadway. *Geomechanics and Engineering*. 2016;11(3):401–420.
33 Yang SQ, Chen M, Jing HW, Chen KF, Meng B. A case study on large deformation failure mechanism of deep soft rock roadway in Xin'An coal mine. *China. Engineering Geology*. 2017;217:89–101.
34 Ghazvinian E, Kalenchuk KS, Diederichs MS. Three-dimensional random Voronoi models for simulation of brittle rock damage around underground excavations in laminated ground. Perth, Australia *Proceedings of Deep Mining*. 2017:277–288.
35 Horino FG, Duvall WI, Brady BT. *The Use of Rock Bolts or Wire Rope to Increase the Strength of Fractured Model Pillars*. U.S. Bureau of Mines Report of Investigation; 1971:1–24. RI-7568.
36 Guana M. *Angle bolts control rib side at No. 4 Mine, Brockwood, Alabama*. Salt Lake City, UT: Proceedings of SME-AIME Fall Meeting and Exhibit; 1983. Preprint number 83-310.
37 Guana M, Mark C. Protecting underground coal miners from rib falls. *Proceedings of the 30th International Conference on Ground Control in Mining, Morgantown, WV*. 2010; 30:126–134.
38 Dolinar DR, Tadolini SC. *Entry Stabilization Using Rib Bolting Procedures*. U.S. Bureau of Mines Report of Investigation; 1991:1–13. RI-9366.
39 Colwell M, Mark C. Analysis and design of rib support (ADRS) – a rib support design methodology for Australian collieries. *Proceedings of the 24th International Conference on Ground Control in Mining, Morgantown, WV*. 2005;24:12–22.
40 Mohamed KM, Tulu IB, Klemetti T. *Numerical simulation of deformation and failure process of coal-mass. Proceedings of the 49th US Rock Mechanics/Geomechanics Symposium*. San Francisco, California: American Rock Mechanics Association; 2015. Paper No. 363.
41 Mohamed KM, Tulu IB, Murphy MM. *Numerical model calibration for simulating coal ribs. Proceedings of the Society for Mining*. Pheonix, Arizona: Metallurgy and Exploration Inc Annual Conference; 2016.
42 Sears MM, Rusnak J, Van Dyke M, Rashed G, Mohamed KM, Sloan M. Coal rib response during bench mining: a case study. *International Journal of Mining Science and Technology*. 2018;28(1):107–113.
43 Zhang P, Mohamed KM, Trackemas J. *Coal rib failure and support in longwall gate entries. Proceedings of the 51th US Rock Mechanics/Geomechanics Symposium*. San Francisco: California; 2017. Paper No. 886.
44 Slaker B, Gangrade V, Murphy MM, Winfield J. *Seismic data interpretation of a development pillar at a steeply dipping underground limestone mine*. Seattle, WA. *Proceedings of the 52nd US Rock Mechanics/Geomechanics Symposium*. 2018. Paper No. 194.
45 Slaker B, Mohamed KM. A practical application of photogrammetry to performing rib characterization measurements in an underground coal mine using a DSLR camera. *International Journal of Mining Science and Technology*. 2017;27(1):83–90.
46 MSHA. *Mining Industry Accident, Injuries, Employment and Production Statistics and Reports*. March 1st; 2019. Retrieved from: https://arlweb.msha.gov/ACCINJ/accinj.htm.
47 Walton G, Sinha S. *Advances in bonded block modeling. Proceedings of Bergmekanikdagen*. Sweden: Swedish Rock Engineering Association; 2020.
48 Sinha S, Walton G. Modeling behaviors of a coal pillar rib using the progressive s-shaped yield criterion. *Journal of Rock Mechanics and Geotechnical Engineering*. 2020; 12(3):484–492.
49 Sinha S, Walton G. A progressive S-shaped yield criterion and its application to rock pillar behavior. *Int J Rock Mech Min Sci*. 2018;105:98–109.
50 Lorig LJ, Varona P. *Guidelines for numerical modelling of rock support for mines. Proceedings of the 7th International Symposium on Ground Support in Mining and Underground Construction*. Australia: Australian Centre for Geomechanics; 2013: 81–105.
51 Gao F. *Simulation of Failure Mechanisms Around Underground Coal Mine Openings Using Discrete Element Modelling*. PhD Dissertation, Simon Fraser University; Canada 2013.
52 Karampinos E, Hadjigeorgiou J, Hazzard J, Turcotte P. Discrete element modelling of the buckling phenomenon in deep hard rock mines. *Int J Rock Mech Min Sci*. 2015;80: 346–356.
53 Gale WJ, Mark C, Oyler DC, Chen J. *Computer simulation of ground behavior and rock bolt interaction at Emerald Mine*. Proceedings of the 23rd International Conference on Ground Control in Mining, Morgantown, West Virginia, USA. 2004:27–34.
54 Zipf RK. Numerical modeling procedures for practical coal mine design. In: *Proceedings of the International Workshop on Rock Mass Classification in Underground Mine Design, NIOSH IC 9498*. 2007:153–162.
55 Mark C, Gale W, Oyler D, Chen J. Case history of the response of a longwall entry subjected to concentrated horizontal stress. *Int J Rock Mech Min Sci*. 2007;44(2): 210–221.
56 Kaiser PK, McCreath D, Tannant D. *Canadian Rockburst Support Handbook*. Geomechanics Research Center and CMIRO Sudbury; Canada 1996.
57 Bouzeran L, Furtney J, Pierce M, Hazzard J, Lemos JV. *Simulation of ground support performance in highly fractured and bulked rock masses with advanced 3DEC bolt model*. Perth, Australia. *Proceedings of the Eighth International Conference on Deep and High Stress Mining*. 2017:667–680.
58 Itasca UDEC. *Version 6.0: Theory and Background*. Minneapolis, Minnesota: Itasca Consulting Group Inc.; 2014.
59 Sinha S, Walton G. Integration of a three-dimensional continuum model and a two-dimensional Bonded Block Model (BBM) for studying the damage process in a granite pillar at the Creighton Mine, Sudbury, Canada. *Journal of Rock Mechanics and Geotechnical Engineering*. 2021;13(2):275–288.
60 Hajiabdolmajid V, Kaiser PK, Martin CD. Modelling brittle failure of rock. *Int J Rock Mech Min Sci*. 2002;39(6), 731–341.
61 Martin CD, Chandler NA. The progressive fracture of Lac Du Bonnet granite. *Int J Rock Mech Min Sci Geomech Abstr*. 1994;31(6):643–659.
62 Kim B, Walton G, Larson MK, Berry S. Investigation of the anisotropic confinement-dependent brittleness of a Utah coal. *International Journal of Coal Science and Technology*. 2021;8(2):274–290. https://doi.org/10.1007/s40789-020-00364-7.
63 Ghazvinian E, Diederichs MS, Quey R. 3D random Voronoi grain-based models for simulating of brittle rock damage and fabric-guided micro-fracturing. *Journal of Rock Mechanics and Geotechnical Engineering*. 2014;6:506–521.
64 Zhu D, Wu Y, Liu Z, Dong X, Yu J. *Failure mechanism and safety control strategy for laminated roof of wide-span roadway*. Engineering Failure Analysis; 2020:104489.
65 Gale WJ. The application of stress measurements to the optimization coal mine roadway drive age in the Illawarra coal measures. Sweden *Proceedings of the ISRM International Symposium*. 1986:551–560.
66 Walsh R. West Cliff longwall outburst–update. *Half day seminar, gas and coal outburst committee, Wollongong*. 1999.
67 Heidbach O, Rajabi M, Reiter K, Ziegler M. *World Stress Map 2016*. GFZ Data Service; 2016.
68 Walton G, Diederichs MS, Punkkinen A, Whitmore J. Back analysis of a pillar monitoring experiment at 2.4 km depth in the Sudbury Basin, Canada. *Int J Rock Mech Min Sci*. 2016;85:33–51.
69 Garza-Cruz TV, Pierce M, Kaiser PK. *Use of 3DEC to study spalling and deformation associated with tunnelling at depth*. Perth, Australia. *Proceedings of the Seventh International Conference on Deep and High Stress Mining*. 2014:421–434.
70 Itasca UDEC. *Version 6.0: Structural Elements*. Minneapolis, Minnesota: Itasca Consulting Group Inc.; 2014.
71 Farmer IW. Stress distribution along a resin grouted rock anchor. *Int J Rock Mech Min Sci Geomech Abstr*. 1975;12(11):347–351.
72 Itasca FLAC. *3D Example Application Version V6*. Minneapolis, Minnesota: Itasca Consulting Group; 2016.
73 Carter TG, Diederichs MS, Carvalho JL. Application of modified Hoek-Brown transition relationships for assessing strength and post yield behaviour at both ends of the rock competence scale. *J S Afr Inst Min Metall*. 2008;108(6):325–338.
74 Edelbro C. Numerical modelling of observed fallouts in hard rock masses using an instantaneous cohesion-softening friction-hardening model. *Tunn Undergr Space Technol*. 2009;24(4):398–409.
75 Renani HR, Martin CD. Modeling the progressive failure of hard rock pillars. *Tunn Undergr Space Technol*. 2018;74:71–81.
76 Wagner H. *Determination of the complete load-deformation characteristics of coal pillars*. Washington, DC: Proceedings of the 3rd International Congress Rock Mechanics; 1974:1076–1081.
77 Esterhuizen E, Mark C, Murphy MM. Numerical model calibration for simulating coal pillars, gob and overburden response. *Proceeding of the 29th International Conference on Ground Control in Mining, Morgantown, WV*. 2010:46–57.
78 Hyett A, Spearing AJ. *New technology for measuring the in-situ performance of rock bolts*. Proceedings of 46th US Rock Mechanics/Geomechanics Symposium, Chicago, Illinois. 2012. Paper No. 497.
79 Walton G. *Improving Continuum Models for Excavations in Rock Masses under High Stress through an Enhanced Understanding of Post-yield Dilatancy*. Kingston, Canada: Ph.D. Thesis. Queen's University; 2014.

80 Oliveira D, Diederichs M. Tunnel support for stress induced failures in Hawkesbury Sandstone. *Tunn Undergr Space Technol*. 2017;64:10–23.
81 Timoshenko SP, Gere JM. *Theory of Elastic Stability*. Courier Corporation; 2009.
82 Seedsman R. *Joint structure and coal strength as controls on rib stability*. *Proceedings of Underground Coal Operators' Conference*. Wollongong, Australia: University of Wollongong; 2006:44–47.
83 Damjanac B, Board M, Lin M, Kicker D, Leem J. Mechanical degradation of emplacement drifts at Yucca Mountain—a modeling case study: Part II: lithophysal rock. *Int J Rock Mech Min Sci*. 2007;44(3):368–399.
84 Wang X, Wu Y, Li X, Liang S. Numerical investigation into evolution of crack and stress in residual coal pillars under the influence of longwall mining of the adjacent underlying coal seam. *Shock Vib*. 2019:2094378.
85 Fabjan T, Mas Ivars D, Vukadin V. Numerical simulation of intact rock behaviour via the continuum and Voronoi tesselletion models: a sensitivity analysis. *Acta Geotechnica Slovenica*. 2015;12(2):5–23.
86 Dadashzadeh N. *Reliability of stress induced damage predictions in hard rocks with continuum and discontinuum numerical modelling approaches*. Doctoral dissertation, Queen's University; 2020.
87 Mohamed K, Van Dyke M, Rashed G, Sears MM, Kimutis R. Preliminary rib support requirements for solid coal ribs using a coal pillar rib rating (CPRR). *International Journal of Mining Science and Technology*. 2021;31(1):15–22.
88 Carvalho JL, Lawrence KP, Moffitt K, Yetisir M. *Behaviour and realm of application of ubiquitous joint constitutive models – facts and limitations*. New York, USA. *Proceedings of the 53rd US Rock Mechanics/Geomechanics Symposium*. 2019. Paper No. 2147.
89 Abousleiman R, Walton G, Sinha S. Understanding roof deformation mechanics and parametric sensitivities of coal mine entries using the discrete element method. *International Journal of Mining Science and Technology*. 2020;30(1):123–129.